Modeling of 980 nm and 1470 nm Laser Radiation Absorbance Efficiency in the Blood Vessel Depending on the Structure of Titanium–Containing Optothermal Fiber Converter

Do Thanh Tung, Andrey V. Belikov, and Yulia V. Semyashkina*
ITMO University, 49 Kronverksky av., Saint Petersburg 197101, Russian Federation

* **e-mail:** yvsemyashkina@mail.ru

Abstract. Using quartz fiber with titanium-containing optothermal fiber converter (TOTFC) is promising in endovenous laser coagulation (EVLA) for the treatment of varicose veins. This study aims to research the variation in the optical properties of TOTFC as its microstructure changes under the condition that TiO_2 spheres inside converter are arranged in such a way that the Mie theory approximation can be applied. The absorbance efficiency of laser energy with 980 nm and 1470 nm wavelengths for TOTFC has been calculated. Optical multidimensional simulation for the EVLA process was developed and calculated. The optimal ranges of microstructure's parameters for TOTFC in the EVLA process were discussed. © 2021 Journal of Biomedical Photonics & Engineering.

Keywords: titanium; optical fiber; varicose vein; blood; optical properties; converter.

Paper #3399 received 31 Dec 2020; revised manuscript received 10 May 2021; accepted for publication 14 May 2021; published online 20 May 2021. doi: 10.18287/JBPE21.07.020304.

1 Introduction

Optothermal fiber converter (OTFC) generated on the distal end of the quartz fiber combined with a laser source has shown advantages for medical surgeries [1]. The use of such converters makes it possible to efficiently process (coagulate, cut, evaporate, etc.) soft biological tissues at different laser wavelengths of laser radiation [2]. Researchers have also confirmed the OTFC is highly effective in the treatment of soft tissue [3, 4]. One of their recent prospects is used in the treatment of varicose veins by endovasal laser coagulation (EVLA) method.

Widely known for treating varicose veins, EVLA uses a puncture in the vein and inserts quartz fiber into the vein. After the laser source is turned on at the suitable wavelength, the fiber is pulled at a speed of several mm/s [5]. Laser radiation with different wavelengths including 980 nm and 1470 nm is used for endovasal laser coagulation [6, 7]. Of course, an anesthetic is injected during the procedure to avoid causing pain to the patient. As a result of laser radiation interactions, the vein vessel wall is heated up to 80 °C and above, that leads to collagen fiber deformation, coagulation, and collapse of the vein [8]. When clear quartz fiber is used, a carbon layer is formed at the tip due to carbonized blood and can be heated to 1200 °C [9, 10]. The high temperature of the tip will easily lead to damage on the vein wall vessel, at the same time, the tip of the fiber is often deformed and broken down. One promising solution to overcome is to use the OTFC on the distal end of optical fiber.

Many types of converters have been fabricated for effective transformation of laser radiation to the heat [11, 12]. Among them, there is the titanium-containing optothermal fiber converter (TOTFC), which is created using of original technology based on 3-stage process. Fabrication technology and structure of TOTFC are described in detail in studies [11, 13] with the microstructure is made up of homogeneous TiO_2 spheres immersed in silica medium. TOTFC shows its good advantages and more suits to other materials in the EVLA process. Using quartz fiber optics with TOTFC makes it easy to control the input parameters in EVLA to help the temperature on the vessel wall reach 80 °C and minimize damage [13–15]. TOTFC has a spherical shape with a smooth surface that makes it easy to put quartz fiber with converter inside blood vessels without causing damage.

Besides, TOTFC is resistant to deformation when laser-heated, as it is capable of being heated up to 2700 °C in air without being destroyed [11]. TOTFC has a strong mechanical connection with optical fiber [11]. Unfortunately, the correlation between the microstructure of TOTFC and its optical properties, as well as the influence of this microstructure to the absorption in converter and in blood vessel of laser radiation with 980 nm and 1470 nm wavelengths of lasers widely used in EVLA has not been studied [7, 10, 15, 16]. We believe that wavelength for EVLA will be a wavelength for which the absorption in the converter will be maximum. On the one hand, this will reduce the power of the laser source necessary for the converter to reach the specified temperature (enough for EVLA), and, on the other hand, it will reduce the risk of unwanted radiation exposure to the vessel wall because laser radiation is not absorbed in the converter, that will lead to an increase in the efficiency and safety of the procedure.

The aim of this study is to find out and evaluate the dependence of TOTFC's optical parameters and light absorbance efficiency at 980 nm and 1470 nm wavelengths on microstructure of converter when the distribution of the TiO_2 spheres inside the converter allows one to apply an approximation of the Mie theory, evaluate the possibility to appear of radiation on the inner vessel wall surface for these two wavelengths in the EVLA procedure and determine the possible optimal for EVLA at 980 nm and 1470 nm wavelengths the parameters of microstructures of TOTFC.

2 Materials and methods

The TOTFC fabrication technology is described in detail in the studies [11, 13]. As the result of fabrication according to this technology, TOTFC is composed of titanium dioxide (TiO_2) spheres with a constant diameter of 1.2 μm and surrounded by silica (SiO_2), forming cubes of equal size (Fig. 1a). The converter has a strong mechanical connection to a quartz fiber of 440 μm diameter.

The volume fraction of spheres in medium (k) characterizes changes in the microstructure of TOTFC is defined by formula:

$$k = \frac{V_{TiO_2}}{V_{cube}} = \frac{\pi d_{sph}^{\ 3}}{6e^3} \qquad (1)$$

where d_{sph} – the diameter of the TiO_2 sphere (constant and equals 1.2 μm), e is a side dimension of the cube.

The microstructure of TOTFC will change if the value k changes, the volume of silica will decrease as k increases. Examples of the microstructures of TOTFC for different values of k are shown in Fig. 1b. When $k = 0$, at this time TOTFC will be completely quartz.

Mie scattering theory is the scattering theory of electromagnetic waves by homogeneous spheres used to calculate the optical properties of materials or substances containing particles in many cases, and its approximation has been confirmed by experimental measurement [17, 18]. Even the particles are not necessarily spherical as in the study [19], and they are not perfectly uniformly arranged in the medium, or in other words, the distance between particles is different. Likewise, TOTFC was generated with homogeneous TiO_2 spheres that were relatively uniformly distributed in silica medium. The ratio of the volume of TiO_2 to silica is one of the standards in TOTFC fabrication. As mentioned above about the structure of TOTFC, by dividing TOTFC's volume by the number of TiO_2 particles, it is easy to find out the structure of a silica cube containing a single TiO_2 sphere embedded within it (as shown in the Fig. 1b).

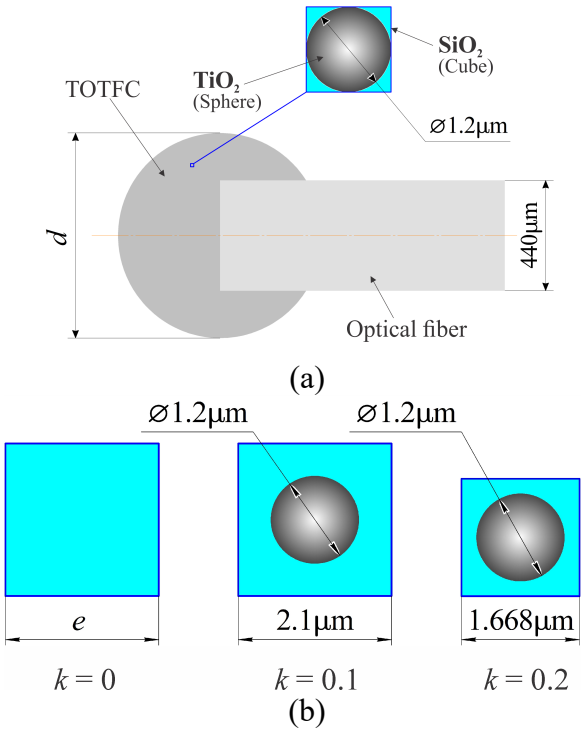

Fig. 1 Structural model of TOTFC (a) and illustration of microstructural changes for various volume fraction of spheres (k) in TOTFC (b).

Since the sphere's diameter (d_{sph} = 1.2 μm) has a value approximately equal to the wavelengths of laser radiation (980 nm and 1470 nm), therefore, to calculate the absorption, scattering, and anisotropy coefficients of TOTFC, we consider using Mie scattering theory [20, 21].

It is well known that scattering by small spheres is well predicted by Mie theory when a sphere is isolated or the distance between the spheres is large enough [22, 23]. This particular kind of scattering is called independent scattering. In this case, intensity scattered by sparse particles can be considered without regard to the phase of the scattered wave. Therefore, it is possible to study scattering by a small particle that is not affected by other particles [24, 25]. Contrary, when the particles are close enough together, the kind of scattering is called dependent scattering, then investigating the scattering for

the spheres cannot ignore the interaction between them, especially the scattering angle [26–28].

According to study [29], using a discrete dipole approximation has shown the criterion for independent scattering when the following condition are met:

$$\frac{h}{a} \geq \frac{2}{x}, \tag{2}$$

where h – distance between the particles (surface to surface), a – radius of each sphere, x – sphere size parameter is defined as:

$$x = \frac{2\pi a}{\lambda}. \tag{3}$$

Thus, for $\lambda = 980$ nm the independent scattering approximation is satisfied at $k \leq 0.26$, and for $\lambda = 1470$ nm the independent scattering approximation is satisfied at $k \leq 0.2$. A task about independent scattering particles has also been theoretically calculated and experimentally carried out in Ref. [30] up to a volume particle concentration of 0.227, although the wavelength of the incident rays is 1.5 times greater than the diameter of particles. The computation of the electromagnetic waves transferred under dependent scattering condition when k is outside the above ranges is complex, and it is out of the scope of this paper. Following Liou in Ref. [24], a complementary theory of Mie scattering has been developed for a sample of spherical particles under independent scattering condition. Whereby, when the minimum radius of particles a_1 is asymptotic to the maximum radius a_2, the scattering phase matrix for a sample of particles is equal to the scattering phase matrix for an isolated particle. In other words, when the radius of all spheres is similar, the scattering intensity of a sample of particles can be calculated by predicting for an isolating sphere. Therefore, with the above description of the TOTFC microstructure, Mie scattering theory can be applied if $k \leq 0.26$ for $\lambda = 980$ nm and $k \leq 0.2$ for $\lambda = 1470$ nm.

According to the formula given in studies [20, 21, 32], TOTFC's optical properties are defined by:

$$\mu_s = \frac{1}{4}\pi d_{sph}^2 Q_{abs}, \tag{4}$$

$$\mu_s = \frac{1}{4}\pi d_{sph}^2 Q_{sca}, \tag{5}$$

$$Q_{ext} = Q_{sca} + Q_{abs}, \tag{6}$$

where μ_a, μ_s – the absorption and scattering coefficients of TOTFC, respectively. Q_{sca} – the scattering efficiency follows from the integration of the scattered power over all directions, and Q_{ext} – the extinction efficiency follows from the Extinction Theorem, leading to:

$$Q_{sca} = \frac{2}{\alpha^2}\sum_{n=1}^{\infty}(2n+1)\left(|a_n|^2 + |b_n|^2\right), \tag{7}$$

$$Q_{ext} = \frac{2}{\alpha^2}\sum_{n=1}^{\infty}(2n+1)\,\mathrm{Re}\left(a_n + b_n\right), \tag{8}$$

note that:

$$\alpha = \frac{\pi m d_{sph}}{\lambda}, \tag{9}$$

where m is the refractive indices of the host medium (here is silica), a_n and b_n are Mie coefficients, function $\mathrm{Re}(a_n + b_n)$ represents the real part of the argument.

Based on the previously defined volume fractions of titanium dioxide k, together with the library of refractive index constants of TiO_2 and SiO_2 [31], we can calculate the refractive index of TOTFC depending on the value k. Then, using the tools of program "MATLAB" (MathWorks, USA) [32] and with the help of Scott Prahl given in Ref. [33], the absorption, scattering, and anisotropy coefficients of TOTFC were determined.

In the EVLA process, the temperature interacts to the blood vessel wall is mainly due to the absorbed laser radiation at TOTFC and heating it up. To calculate the TOTFC's light absorbance efficiency (A), a simulation model of the EVLA procedure is created in environment 3-dimensional space configuration "TracePro® Expert-7.0.1 Release" ("Lambda Research Corporation", USA), shown in Fig. 2.

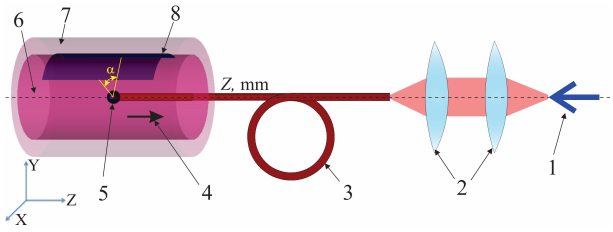

Fig. 2 EVLA procedure model; 1 – laser source; 2 – lenses; 3 – quartz optical fiber; 4 – the direction of movement of fiber and TOTFC; 5 – TOTFC; 6 – blood; 7 – vein wall; 8 – the detector plane which totally absorbs light and located on the inner wall of the vein and limited by an angle α.

Optical modeling was performed by Monte Carlo simulations of radiative transfer. Laser sources radiation continuously with tracing of 10000 rays, the numerical aperture NA = 0.22. After passing through two focusing lenses, the focused beam passes through a quartz optical fiber 3 m in length. The TOTFC is located at the distal end of the fiber and it is centrally located in a blood vessel 5 mm in inner diameter. The physical parameters of the

vein, quartz fiber and titanium-containing optothermal fiber converter required to construct an optical model were taken in [15, 34, 35] and are represented in Table 1.

Table 1. Physical parameters for laser source, quartz fiber, vein and TOTFC.

Laser source	Optical power	20 W
	Divergence	0.22
Quartz fiber	NA	0.22
	Diameter (core)	0.4 mm
	Diameter (cladding)	0.44 mm
	Length	3 m
	Refractive index (core)	1.457
	Refractive index (cladding)	1.44
Vein	Inner diameter	5 mm
Vein wall	Thickness	1 mm
TOTFC	Thickness/Diameter	0.7 mm/ 0.78 mm

Here, we define TOTFC's diameter as 780 μm, which is similar to the actual dimensions has been fabricated in the study [13]. But during modeling we will change the diameter of TOTFC. The optical parameters of the vein wall and blood for 980 nm and 1470 nm wavelengths are given in studies [6, 36–39], these are shown in Table 2.

Table 2. Optical parameters for vein wall and blood at 980 nm and 1470 nm.

Wavelength [nm]		980	1470
Vein wall	Absorption coefficient [mm^{-1}]	0.22	2.01
	Scattering coefficient [mm^{-1}]	14.8	31
	Anisotropy factor	0.96	0.95
Blood	Absorption coefficient [mm^{-1}]	0.29	2.33
	Scattering coefficient [mm^{-1}]	46.7	27.78
	Anisotropy factor	0.9763	0.9562

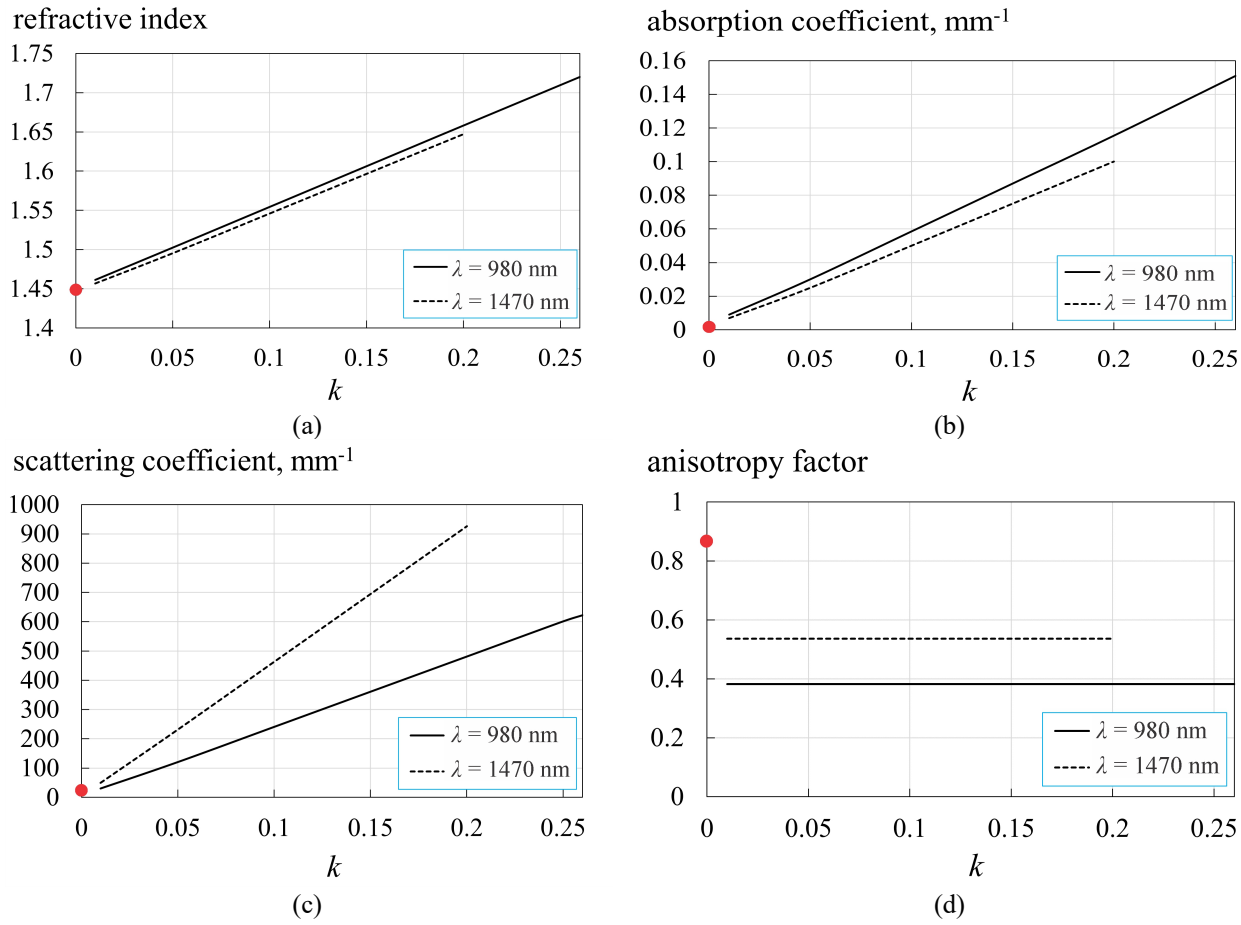

Fig. 3 Dependence of the refractive index (a), absorption coefficient (b), scattering coefficient (c) and anisotropy factor (d) on the volume fraction k of TiO_2 in TOTFC.

3 Results and Discussion

The change of the microstructure in TOTFC as the volume fraction k of TiO_2 shown in Eq. (1) will significantly change the optical properties of TOTFC. Fig. 3 shows the influence of the value k on the optical properties of TOTFC.

Investigate the k ranging from 0.01 to 0.2 for $\lambda = 1470$ nm and from 0.01 to 0.26 for $\lambda = 980$ nm. At a value of $k = 0$, meaning that there is no TiO_2 sphere in the silica cube (see Fig. 1b), in this case, the optical properties of TOTFC are the optical properties of silica (SiO2). In Fig. 3, at $k = 0$, the red spots showing the refractive index, absorption, scattering coefficient, and anisotropy factor of SiO_2 were confirmed in Refs. [31, 40, 41]. It can be seen that when k changes there is not much difference in the refractive index of TOTFC between 980 nm and 1470 nm wavelengths. They both increase linearly with the increasing of the value k. For the refractive index of SiO_2 corresponding to $k = 0$, the red point in this case belongs to the graph line showing the computation certainty (see Fig. 3a). Similar to the dependence of the absorption and scattering coefficient on the volume fraction of TiO_2 (see Fig. 3b, c). The absorption coefficient of silica is very small, equal to 10^{-6} mm^{-1} [40]. The scattering coefficient of silica ranges from 14.6 to 20.2 mm^{-1} [41]. The absorption and scattering coefficients of TOTFC increased as the volume fraction k of TiO_2 increased, because at this time, the number of TiO_2 spheres in the TOTFC would increase, increasing optical absorption and scattering. The absorption coefficient of TOTFC increased with increasing k, but in general, for both wavelengths these values are very small, less than 0.15 mm^{-1}. The scattering coefficient of TOTFC increased strongly with increasing k, with maximum values of 620 mm^{-1} for 980 nm and 930 mm^{-1} for 1470 nm wavelength. The anisotropy factor of TOTFC is unchanged when k is changed, and it only depends on the laser wavelength (see Fig. 3d). This can be explained because the size of the TiO_2 spheres is unchanged. In Fig. 3d, at $k = 0$, the red point represents the magnitude of the anisotropy factor of SiO_2 is equal to 0.88, which was experimented on in research [41]. Comparison between wavelengths 980 nm and 1470 nm show that the scattering coefficient and anisotropy factor of TOTFC for 1470 nm wavelength is the magnitude higher. The anisotropy factor of TOTFC $g = 0.3815$ for 980 nm and $g = 0.5360$ for 1470 nm wavelength.

The diagrams of the absorption and scattering coefficients of TOTFC increased linearly as the volume fraction k increased, consistent with a similar experimental measurement in the study [30]. In there, experiments were measured for the Intralipid with diffused soybean oil particles. In Ref. [30], the scattering coefficient increases non-linearly as k increases close to the maximum value, possibly due to the influence of dependent scattering. A proof of this can be seen in Ref. [28] when the relative between the independent and the dependent scattering is shown. The anisotropy factor g has also been measured in Ref. [30], with a slight decrease as the volume fraction k increased; however, the error of this measurement was so much, up to 8%.

It is generally accepted that during endovasal laser coagulation, optical influence assessment, and further, the distribution of temperature onto the vein wall is crucial [36–38]. According to this, after calculating the optical properties of TOTFC, using "TracePro® Expert-7.0.1 Release" the ray tracing for 980 nm and 1470 nm laser radiation in the blood vessel was done. In Fig. 4, the path of rays through TOTFC placed in the blood vessel for the volume fraction $k = 0.01$ and $k = 0.2$ were obtained.

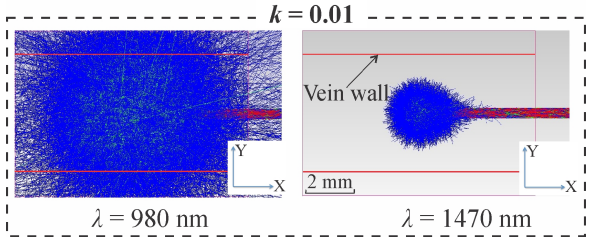

(a)

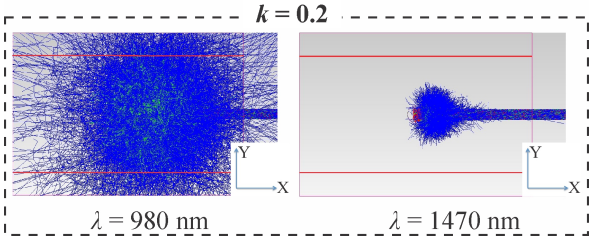

(b)

Fig. 4 Path of rays through TOTFC placed in the blood vessel for the volume fraction $k = 0.01$ (a) and $k = 0.2$ (b) into the YZ plane (X = 0).

As seen in Fig. 4, the distribution of rays leaving the TOTFC for $k = 0.01$ is different with $k = 0.2$ at the same wavelength. This is probably because the absorption and scattering coefficients of TOTFC are gradually increasing as the value k increases (see Fig. 3b, c). Wherein, the change is significant as the laser wavelength changes. It can be observed that laser radiation for 980 nm reaches the vein wall. While laser radiation for 1470 nm is concentrated mostly near the converter, and cannot reach the vein wall, even at all values of k. This can be explained by the fact that the absorption coefficient of blood for 1470 nm is many times of the magnitude larger than that for 980 nm wavelength (see Table 2).

To evaluate the magnitude of 980 nm radiation intensity impacting the blood vessel walls, we used a detector plane which totally absorbs light and located on the inner wall of the vein and limited by an angle $\alpha = 90^{\circ}$ with along Z-axis length equal to 7 mm (see Fig. 2). The distal end of fiber with TOTFC is placed in the position

where the coordinate Z = 0. Fig. 5 shows the radiation intensity distribution on the inner vessel wall surface with $k = 0.01$ and $k = 0.26$ (if laser power equals 20 W).

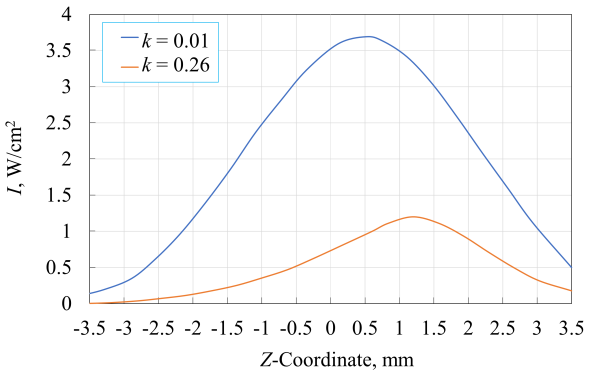

Fig. 5 The distribution of the 980 nm laser radiation intensity (I) on the inner vein wall surface along Z-coordinate with $k = 0.01$ and $k = 0.26$.

The dependence of average 980 nm laser radiation intensity on the inner vessel wall surface on k was determined. It can be seen that the radiation intensity distribution on the inner vein wall surface reaches peak magnitude at a point in the opposite direction to the incident rays. At $k = 0.26$, this peak has a coordinate farther from the TOTFC's center (Z = 0) as compared with $k = 0.01$. This may be due to the increase in the scattering coefficient of TOTFC as the value k increases (see Fig. 3c). The average of laser radiation intensity on the inner vessel wall surface reaches magnitude $I = 3.70$ W/cm^2 for $k = 0.01$ and $I = 1.25$ W/cm^2 for $k = 0.26$. As can be seen, a larger value k will reduce the intensity of radiation on the inner vein wall surface, thereby reducing the risk of unwanted radiation exposure to the vessel wall by laser radiation.

The dependences of TOTFC's light absorbance efficiency (A) and transmission (T) on k and diameter of converter (d) for wavelengths of 980 nm and 1470 nm are shown in Fig. 6.

In general, the TOTFC with volume fraction $k = 0.26$ and $d = 0.78$ mm is optimal with the light absorbance efficiency A of over 83% (see Fig. 6a). However, for TOTFC at $k = 0.15$ we also demonstrated the ability to absorb radiation well with 80% for 980 nm and 82% for 1470 nm wavelength. Using TOTFC at $k = 0.2$, we examined its A and T when the diameter of the TOTFC d was changed (see Fig. 6b).

The transmission is calculated directly by measuring the percentage of the power received around the TOTFC by using a totally absorbing spherical detector. Besides, a detector plane is also placed in front of the source to measure the percentage reflectance of the TOTFC. Then, after subtracting 4% of the Fresnel loss energy at the fiber's input, the radiation is absorbed in quartz fiber, which is 0.3% for 3 m in length [13, 34], from there the rest is the TOTFC's light absorbance efficiency. In accordance with Ref. [40, 42], the transmittance of silica quartz is about 92% for the wavelength range from 0.4 μm to 2 μm for 1 m length, plus the radiation loss due to reflection implies that the absorption of the silica is close to zero. These correspond to the red and blue spots shown in Fig. 6a.

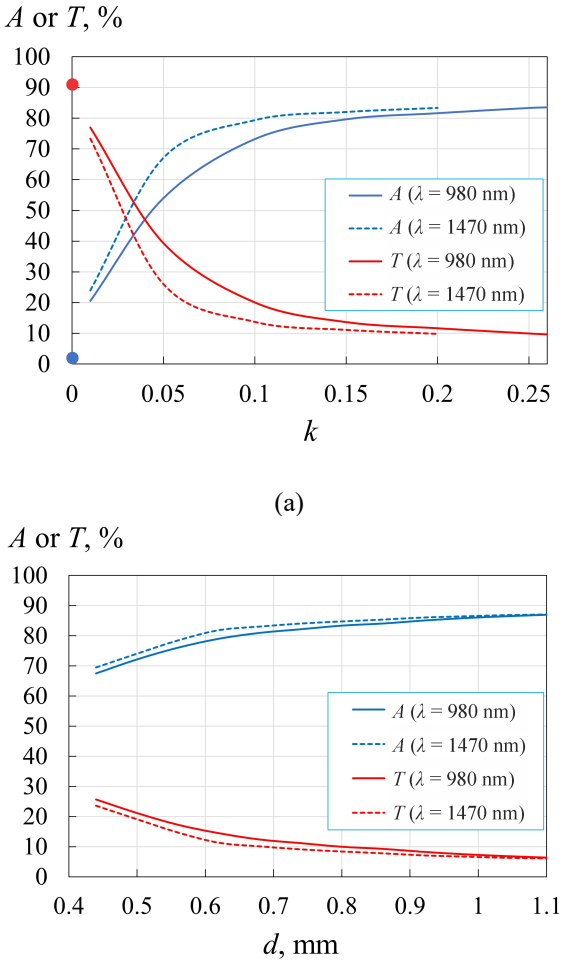

Fig. 6 Dependence of TOTFC's light absorbance efficiency (A) and transmission (T) on the volume fraction k with $d = 0.78$ mm (a) and diameter of converter d with $k = 0.2$ (b) for wavelengths 980 nm and 1470 nm.

It can also be seen that the transmittance of TOTFC (red line) decreases rapidly in the k range from 0.01 to 0.1, then slowly decreases until $k = 0.26$. It is synonymous with that, TOTFC's light absorbance efficiency increases rapidly when k is from 0.01 to 0.1 and reaches maximum magnitude at $k = 0.26$. Apparently, the presence of TiO_2 spheres greatly increased TOTFC's ability to absorb radiation.

In addition, the TOTFC's light absorbance efficiency for 980 nm is the magnitude lower than that for 1470 nm wavelength in the k range of 0.01 to 0.15 and is almost equals when $k > 0.15$. At the value $k = 0.22$, the magnitude of TOTFC's light absorbance efficiency is equal to 83.2% for 980 nm wavelength, agreement with the results in Ref. [13, 15].

Since the diameter of the quartz optic fiber is 0.44 mm, so the minimum diameter of TOTFC is 0.44 mm. Fig. 6b shows the TOTFC's light absorbance efficiency and transmission as the diameter of TOTFC increases from 0.44 mm to 1.1 mm for both wavelengths. TOTFC's light absorbance efficiency increase but gradually slow as the TOTFC's diameter increases. The opposite happens with the transmission. Obviously, when the diameter of the TOTFC increases, it will lead to an increase in its volume, that makes the radiation absorption efficiency of TOTFC to increase.

In summary, the increased diameter of the TOTFC will increase the radiation absorption efficiency and decrease the radiation intensity on the inner vessel wall surface. TOTFC's light absorbance efficiency will be 80% higher when its diameter is greater than 0.67 mm. Therefore, the TOTFC structure with k from range $0.15 \div 0.26$ and $d > 0.67$ mm demonstrates the high enough absorbance efficiency. It should be noted that the diameter d is limited from above by the size of the vein and cannot exceed its inner diameter.

4 Conclusion

The optical properties of TOTFC with different volume fraction k of TiO_2 at wavelengths of 980 nm and 1470 nm of lasers widely used in EVLA are considered when the TiO_2 spheres are sparse enough for the Mie theory approximation application. The optical properties of TOTFC at these wavelengths changed significantly as the microscopic structure of TOTFC changed. The radiation absorption efficiency of TOTFC increases with increasing the volume fraction k up to 0.26 for 980 nm and up to 0.2 for 1470 nm. The results are confirmed based on the known optical properties of silica (SiO_2) and a measurement experiment with independent scattering particles [30]. TOTFC's absorbance efficiency of laser radiation has been calculated. It was clearly evident from the calculated results that absorbance efficiency increased as diameter of converter increased. As a result of optical calculations, radiation intensity distributions on the inner vessel wall surface were investigated. The results also showed that for 1470 nm wavelength, radiation could not reach the vein wall, that is positive as it increases the efficiency and safety of EVLA. The possible optimal for EVLA, microstructures of TOTFC with $0.15 \le k \le 0.26$ for 980 nm and $0.15 \le k \le 0.2$ for 1470 nm wavelengths, and diameter $d > 0.67$ mm because of these ranges of volume fraction and diameter of converter observe the high enough absorbance efficiency of laser radiation for TOTFC (more than 80%). The results of this study will be used in the subsequent thermophysical modeling of laser heating of a vein and can be useful in the development of new laser devices for EVLA.

Disclosures

All authors declare that there is no conflict of interests in this paper.

Acknowledgements

The authors are grateful to ITMO University (Saint Petersburg, Russia) for providing equipment and support to this study. This work was carried out within the framework of the program for improving the competitiveness of ITMO University among the world's leading research and educational centers for 2013–2020 ("5 in 100" program, grant 08-08).

References

1. A. V. Skripnik, "Opto-thermal fiber converter of laser radiation," Journal of instrument engineering 9(56), 37–42 (2013).
2. R. M. Verdaasdonk, C. F. P. Van Swol, "Laser light delivery systems for medical applications," Physics in Medicine and Biology 42, 869–894 (1997).
3. A. V. Belikov, A. V. Skrypnik, and K. V. Shatilova, "Comparison of diode laser in soft tissue surgery using continuous wave and pulsed modes in vitro," Frontiers of Optoelectronics 8(2), 212–219 (2015).
4. A. V. Belikov, A. V. Skrypnik, and V. Y. Kurnyshev, "Modeling of structure and properties of thermo-optical converters for laser surgery," Proceedings of SPIE 9917, 99170G (2015).
5. Yu. L. Shevchenko, K. V. Mazaishvili, and Yu. M. Stoiko, Laser Surgery for Varicose Vein Disease, Borges, Moscow (2010) [in Russian]. ISBN: 978-5-9902607-1-9.
6. A. A. Poluektova, W. S. J. Malskat, M. J. C. van Gemert, M. E. Vuylsteke, C. M. A. Bruijninckx, H. A. Martino Neumann, and C. W. M. van der Geld, "Some controversies in endovenous laser ablation of varicose veins addressed by optical-thermal mathematical modeling," Lasers in Medical Science 29(2), 441–452 (2014).
7. R. R. Van Den Bos, P. W. M.van Ruijven, C. W. M. van der Geld, M. J. C. van Gemert, H. A. M. Neumann, and T. Nijstena, "Endovenous simulated laser experiments at 940 nm and 1470 nm suggest wavelength-independent temperature profiles," European Journal of Vascular and Endovascular Surgery 44(1), 77–81 (2012).
8. E. V. Shaydakov, E. A. Iluhin, Endovascular methods in the treatment of varicose veins, Diton-Art, Saint Petersburg (2016).
9. Yu. L. Shevchenko, Yu. M. Stoyko, K. V. Mazayshvili, and T. V. Khlevtova, "The mechanism of endovenous laser obliteration: a new look," Phlebology 5(1), 46–50 (2011) [in Russian]. ISBN: 978-5-905048-97-5.

10. M. Amzayyb, R. R. van den Bos, V. M. Kodach, D. M. de Bruin, T. Nijsten, H. A. M. Neumann, and M. J. C. van Gemert, "Carbonized blood deposited on fibres during 810, 940 and 1,470 nm endovenous laser ablation: thickness and absorption by optical coherence tomography," Lasers in Medical Science 25(3), 439–447 (2010).
11. A. V. Belikov, A. V. Skrypnik, "Laser heating dynamics and glow spectra of carbon-, titanium- and erbium-containing optothermal fibre converters for laser medicine," Quantum Electronics 47(7), 669−674 (2017).
12. A. V. Belikov, A. V. Skrypnik, "Soft tissue cutting efficiency by 980 nm laser with carbon-, erbium-, and titanium-doped optothermal fiber converters," Lasers in Surgery and Medicine 51(2), 185−200 (2019).
13. A. V. Belikov, A. V. Skrypnik, and I. S. Salogubova, "Optical and thermal modeling of Ti-doped optothermal fiber converter for laser surgery," Proceedings of SPIE 11065, 1106514 (2019).
14. A. V. Belikov, T. Do, and Yu. V. Semyashkina, "Laser heating numerical simulation of titanium-containing optothermal fiber converter and vein wall during endovasal laser coagulation," Scientific and Technical Journal of Information Technologies, Mechanics and Optics 20(4), 485–493 (2020).
15. A. V. Belikov, T. Do Thanh, A. V. Skrypnik, and Y. V. Semyashkina, "Modeling of optothermal fiber converters interaction with vein during endovenous laser coagulation," Proceedings of SPIE 11457, 114571L (2020).
16. M. Vuylsteke, J. V. Dorpe, J. Roelens, Th. D. Bo, and S. Mordon, "Endovenous laser treatment: a morphological study in an animal model," Phlebology 24(4), 166–175 (2009).
17. T. Wriedt, "Mie theory: a review," The Mie Theory 169, 53–71 (2012).
18. J. M. Steinke, A. P. Shepherd, "Comparison of Mie theory and the light scattering of red blood cells," Applied Optics 27(19), 4027–4033 (1988).
19. P. K. Jain, K. S. Lee, I. H. El-Sayed, and M. A. El-Sayed, "Calculated absorption and scattering properties of gold nanoparticles of different size, shape, and composition: applications in biological imaging and biomedicine," The journal of physical chemistry B 110(14), 7238–7248 (2006).
20. W. C. Mundy, J. A. Roux, and A. M. Smith, "Mie scattering by spheres in an absorbing medium," JOSA 64(12), 1593–1597 (1974).
21. Q. Fu, W. Sun, "Mie theory for light scattering by a spherical particle in an absorbing medium," Applied Optics 40(9), 1354–1361 (2001).
22. C. F. Bohren, D. R. Huffman, Absorption and scattering of light by small particles, Wiley, New York, USA (1983).
23. H. C. van de Hulst, Light scattering by small particles, Dover Publications, New York, USA (1981).
24. K. N. Liou, "A complementary theory of light scattering by homogeneous spheres," Applied Mathematics and Computation 3(4), 331–358 (1977).
25. M. I. Mishchenko, J. W. Hovenier, and L. D. Travis (Eds.), "Concepts, terms, notation," Chapter 1 in Light Scattering by Nonspherical Particles, 3–27 (2000).
26. J. D. Cartigny, Y. Yamada and C. L. Tien, "Radiative Transfer With Dependent Scattering by Particles: Part 1–Theoretical Investigation," Journal of Heat Transfer 108(3), 608–661 (1986).
27. L. X. Ma, J. Y.Tan, J. M. Zhao, F. Q. Wang, and C. A. Wang, "Multiple and dependent scattering by densely packed discrete spheres: Comparison of radiative transfer and Maxwell theory," Journal of Quantitative Spectroscopy and Radiative Transfer 187, 255–266 (2017).
28. G. Göbel, J. Kuhn, and J. Fricke, "Dependent scattering effects in latexsphere suspensions and scattering powders," Waves in Random Media 5(4), 413–426 (2006).
29. Z̆. Ivezić, M. P. Mengüç, "An investigation of dependent/independent scattering regimes using a discrete dipole approximation," International Journal of Heat and Mass Transfer 39(4), 811–822 (1996).
30. G. Zaccanti, S. Del Bianco, and F. Martelli, "Measurements of optical properties of high-density media," Applied Optics 42(19), 4023–4030 (2003).
31. Refractive index database (accessed 1 December 2020). [https://refractiveindex.info/?shelf=main&book=TiO2&page=Devore-o].
32. C. Mätzler, MATLAB functions for Mie scattering and absorption, version 2, Bern, Switzerland (2002).
33. S. Prahl, Mie Scattering Calculator (accessed 1 December 2020). [https://omlc.org/calc/mie_calc.html].
34. Buffered Fiber Optics, Edmund Optics (accessed 1 December 2020). [http://www.edmundoptics.com/optics/fiber-optics/buffered-fiber-optics/2456].
35. E. Péry, W. C. P. M. Blondel, J. Didelon, A. Leroux, and F. Guillemin, "Simultaneous characterization of optical and rheological properties of carotid arteries via bimodal spectroscopy: Experimental and simulation results," IEEE Transactions on Biomedical Engineering 56(5), 4760278, 1267–1276 (2009).
36. M. Hirokawa, T. Ogawa, H. Sugawara, S. Shokoku, and S. Sato, "Comparison of 1470 nm laser and radial 2ring fiber with 980 nm laser and bare-tip fiber in endovenous laser ablation of saphenous varicose veins: a multicenter, prospective, randomized, non-blind study," Annals of Vascular Diseases 8(4), 282–289 (2015).
37. P. W. van Ruijven, A. A. Poluektova, M. J. C. van Gemert, H. A. M. Neumann, T. Nijsten, and C. W. M. van der Geld, "Optical-thermal mathematical model for endovenous laser ablation of varicose veins," Lasers in Medical Science 29, 431–439 (2014).
38. S. Nozoea, N. Honda, K. Ishii, and K. Awazu, "Quantitative analysis of endovenous laser ablation based on human vein optical properties," Proceedings of SPIE-OSA Biomedical Optics, 80921J (2011).

39. N. Bosschaart, G. J. Edelman, M. C. G. Aalders, T. G. van Leeuwen, and D. J. Faber "A literature review and novel theoretical approach on the optical properties of whole blood," Lasers in Medical Science 29, 453–479 (2014).
40. "Silica Glass (SiO_2)," Crystran (accessed 1 December 2020). [https://www.crystran.co.uk/optical-materials/silica-glass-sio2].
41. K. Fujiwara, T. Maruyama, S. Nakamura, K. Nitta, and O. Matoba, "Measurement of scattering coefficient in PMMA with SiO2 particles by optical coherence tomography," 17th Microoptics Conference (MOC' 11), 1–2 (2011).
42. Technical Note: Optical Materials, Newport Corporation (accessed 1 December 2020). [https://www.newport.com/n/optical-materials].